

Regression-based Physics Informed Neural Networks (Reg-PINNs) for Magnetopause Tracking

Po-Han Hou

National Central University

kozak20010716@g.ncu.edu.tw

Jih-Hong Shue

National Central University

jhshue@jupiter.ss.ncu.edu.tw

Abstract

The ultimate goal of studying the magnetopause position is to accurately determine its location. Both traditional empirical computation methods and the currently popular machine learning approaches have shown promising results. In this study, we propose a Regression-based Physics-Informed Neural Networks (Reg-PINNs) that combines physics-based numerical computation with vanilla machine learning. This new generation of Physics Informed Neural Networks overcomes the limitations of previous methods restricted to solving ordinary and partial differential equations by incorporating conventional empirical models to aid the convergence and enhance the generalization capability of the neural network. Compared to Shue et al. [1998], our model achieves a reduction of approximately 30% in root mean square error. The methodology presented in this study is not only applicable to space research but can also be referenced in studies across various fields, particularly those involving empirical models.

1 Introduction

Over the past 50 years, various theories have been developed for the boundary between the Earth's magnetosphere and the solar wind, also known as the magnetopause. These include Schield's investigation of the pressure balance between the magnetosphere and the solar wind in 1969 (Schield, 1969), as well as the empirical model for the magnetopause proposed by Shue in 1997 and 1998, which has become the most widely used approach in the past 25 years. Furthermore, Wang *et al.*, 2013 introduced a method using support vector regression (SVR) to calculate the position of the magnetopause. Previous research, whether traditional empirical models or modern machine learning approaches, have their own inherent limitations. Traditional empirical models excel in generalization but sacrifice high precision, while machine learning models achieve excellent precision during training but may not

possess comparable generalization capabilities to empirical models. Therefore, the aim of this study is to integrate the advantages of both approaches and propose a novel form of fitting algorithm called Regression-based Physics Informed Neural Networks, hereafter referred to as Reg-PINNs. This algorithm draws inspiration from Physics Informed Neural Networks (PINNs), which have been developed in the past for high-resolution time evolution simulations or spatial state simulations of real-world physical phenomena using ordinary differential equations (ODEs) and partial differential equations (PDEs). Currently, there is scarce literature on the utilization of algebraic equations for training PINNs. In the second part of this paper, we will present the in-situ traversing data of the magnetopause obtained from multiple satellites that were used in this study. The third part will introduce the modified empirical model and the algorithm for Reg-PINNs. In the fourth part, we will showcase our implementation results, followed by discussions and conclusions.

2 Dataset Preprocessing

A total of 34,998 magnetopause in-situ crossing data points were included in the analysis, derived from various sources such as THEMIS (28,634), Geo-Tail (5,764), ISEE, IMP 8, among others. For each data point, the corresponding time stamps were identified, and the 5-minute averages were calculated using the OMNI dataset recorded at five-minute intervals. In order to enable the empirical model to generalize within a specific region, we integrated the collected data from the same bin. Each bin encompasses north-south interplanetary magnetic field (IMF Bz) values spanning across 3 values, with a shift of 1 Bz for each subsequent bin. Additionally, each bin includes 2 values of solar wind dynamic pressure (Dp), with a shift of 0.5 Dp for each subsequent bin. The range of the dataset used in this study is consistent with that of Shue et al. [1998], which is $-18 < B_z < 15$ and $0.5 < D_p < 8.5$. Figure 1 displays the distribution of X-GSM and Y-GSM coordinates in the GSM coordinate system for the Geo-Tail data. On the other hand, Figure 2 illustrates the range of distribution for Dp and Bz variables.

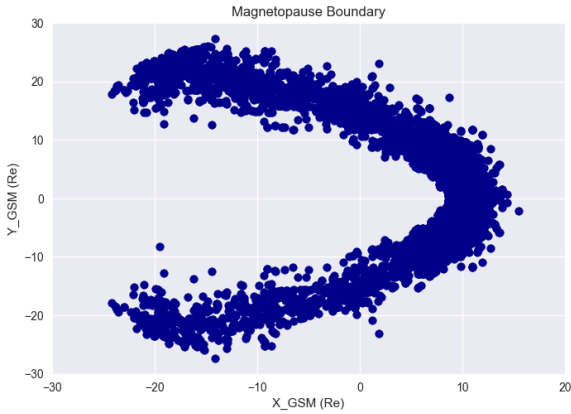


Figure 1. The Geo-Tail satellite crosses the magnetopause at various positions.

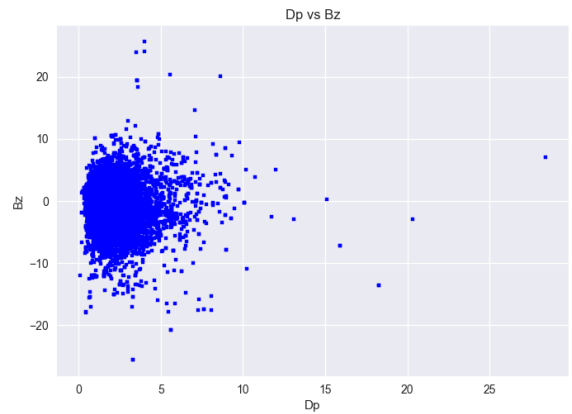


Figure 2. The distribution relationship between Dp and Bz variables

3 Methodologies

There have been numerous studies discussing the construction of empirical models for magnetopause location, including notable works by Roelof and Sibeck, 1993, Shue *et al.*, 1997, Shue *et al.*, 1998, and Chao *et al.*, 2002. In comparison to machine learning approaches, empirical models generally exhibit advantages in terms of generalization ability, although they may lack the precision achieved by machine learning methods. On the other hand, while machine learning demonstrates considerable accuracy, its generalization capability is not significantly improved. Therefore, the inspiration for our proposed model stems from combining the strengths of both approaches, aiming to develop a model that achieves high accuracy and excellent generalization capability.

The fitting of the magnetopause position, as shown in Figure 3, in this study adopts the formulation proposed by Shue *et al.* [1997] as expressed in equation (1) and incorporates the parameters from Shue *et al.* [1998] as the baseline, as shown in equation (2). Subsequently, we will employ neural networks for the fitting process and introduce a novel form of Physics Informed Neural Networks (PINNs) that incorporates empirical equations in the form of algebraic equations. This novel approach is referred to as Regression-based Physics Informed Neural Networks (Reg-PINNs).

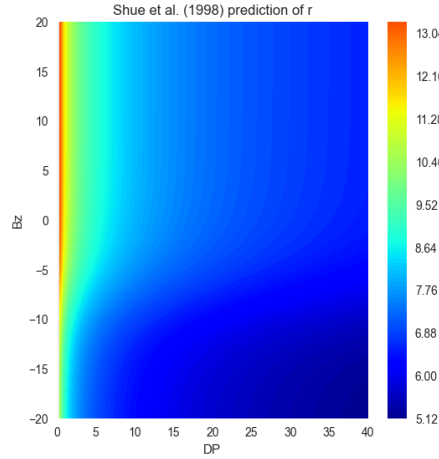


Figure 3. Shue *et al.* [1998] prediction of r

Figure 3 clearly illustrates a significant variation when B_z transitions from -10 to 0. This segment can be explained as the southward interplanetary magnetic field reconnecting on the dayside, subsequently compressing and pushing towards the magnetopause in the direction of Earth.

- Shue *et al.* [1997]

$$r(B_z, Dp, \theta) = r = r_0 \left(\frac{2}{1 + \cos\theta} \right)^\alpha \quad (1)$$

- Parameters from Shue et al. [1998]

$$\begin{aligned} r_0(B_z, D_p) &= r_0 = (10.22 + 1.29 \cdot \tanh(0.184(B_z + 8.14))) (D_p)^{-\frac{1}{6.6}} \\ \alpha(B_z, D_p) &= \alpha = (0.58 - 0.007 \cdot B_z)(1 + 0.024 \cdot \ln(D_p)) \end{aligned} \quad (2)$$

The parameters from Shue et al. [1998] have an accepted range of $-18 < B_z < 15$ and $0.5 < D_p < 8.5$.

3.1 Empirical Method

Shue's model incorporates data from satellites such as ISEE, AMPTE/IRM, and IMP 8, and employs traditional numerical analysis techniques for individual analysis of multivariate inputs. It is known that the magnetopause position is primarily influenced by the B_z and D_p , while the distance from the magnetopause to the Earth serves as the dependent variable. Therefore, Shue utilizes the distance relative to the Earth's magnetopause, along with B_z , D_p , and the angle between the Earth-Sun connection, in his model. The most significant difference in the fitting of the parameters compared to Shue's original formulation is the decay of r_0 relative to B_z when B_z is greater than 0, as shown in Figure 4 and Figure 5. This phenomenon was not observed in Shue's dataset, and thus, Shue et al. [1998] utilized a single hyperbolic tangent function for curve fitting. However, in this study, using the same THEMIS satellite dataset, Nemecek *et al.*, 2010 and Li, Sun and Chen, 2023 have discovered this phenomenon. Therefore, we have reevaluated and modified the original parameter formulation to employ two hyperbolic tangent functions for fitting purposes. We performed individual fitting of each variable using the least squares method employed by Shue. The results are as follows, referring to equation (3) and figure 6:

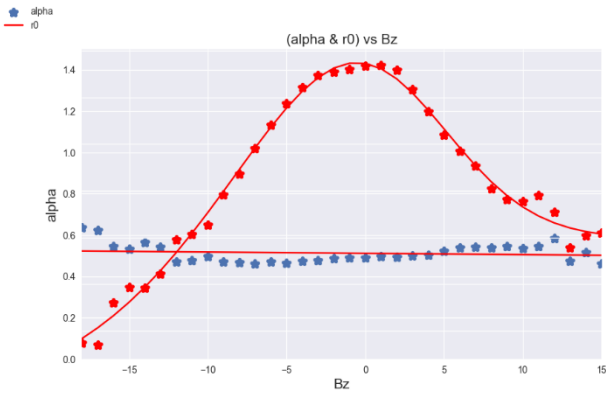


Figure 4. The relationship between α , r_0 , and IMF B_z

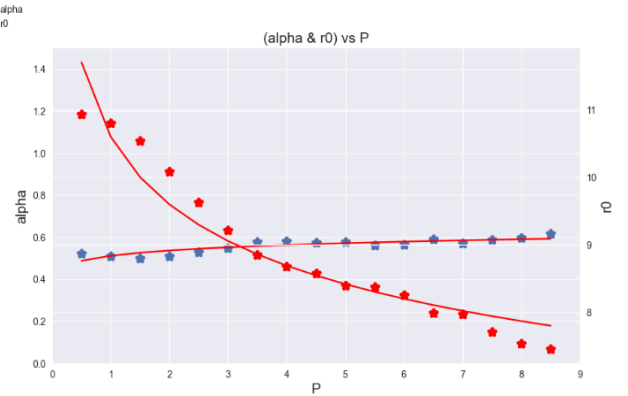


Figure 5. The relationship between α , r_0 , and D_p

$$\begin{aligned} r_0(B_z, D_p) &= r_0 = \left(\begin{aligned} &9.332 + 1.308 \cdot \tanh(0.213(B_z + 11.191)) \\ &- 0.568 \cdot \tanh(0.479(B_z - 7.188)) \end{aligned} \right) (D_p)^{\left(-\frac{1}{6.22}\right)} \\ \alpha(B_z, D_p) &= \alpha = (0.493 - 3.5 \cdot 10^{-4} \cdot B_z)(D_p)^{\left(\frac{1}{11.92}\right)} \end{aligned} \quad (3)$$

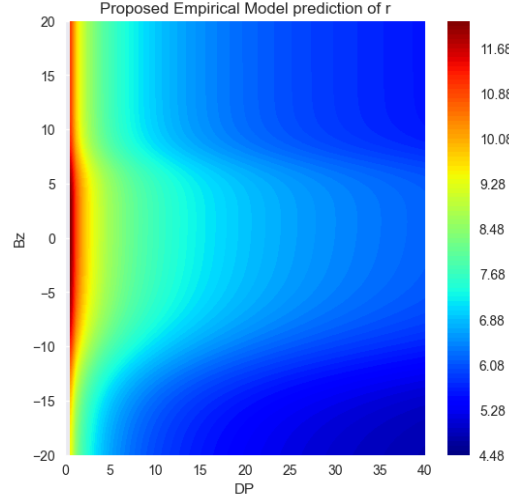


Figure 6. Proposed Empirical Model prediction of r

It is worth noting that the power law relationship between Dp and r_0 , as mentioned by Schield in 1996, refers to the case of an ideal dipole magnetic field in a vacuum, where the relationship between the magnetopause boundary position r_0 and the solar wind dynamic pressure Dp should follow a negative exponential power law with an exponent of $1/6$. This value serves as a reference for comparing the actual relationship between r_0 and Dp under realistic conditions. Shue, on the other hand, calculated an exponent of $1/6.6$ in 1998, while in this study, the calculated exponent is $1/6.22$. In addition, we also employed Markov Chain Monte Carlo (MCMC), which is a commonly used method for parameter estimation and model validation. Its basic idea is to simulate the probability distribution in the parameter space through random selection and sampling, thereby solving unknown parameters of the model. MCMC algorithms mainly include the Metropolis-Hastings algorithm and Gibbs sampling algorithm, among which the Metropolis-Hastings algorithm is a general MCMC algorithm capable of solving parameter estimation problems in any dimension (Speagle, 2020). In our experiment, we obtained promising results using the MCMC approach with 10,000 iterations to extract 11 parameters with the smallest errors.

3.2 Neural Networks

Neural networks have been used for fitting purposes for many years, with the Universal Approximation Theorem (Tianping Chen and Hong Chen, 1995) being the main theoretical support for using machine learning in fitting tasks. The primary objective of implementing neural networks is to project a high-dimensional manifold of features onto the desired solution. The term "universal" signifies that regardless of the mathematical expression $y = f(x)$ that needs to be solved, regardless of the pattern of $f(x)$, a neural network can approximate a solution model that conforms to the desired spatial features; in other words, it can approximate any continuous function to arbitrary accuracy on a compact input domain. Mathematically, it can be expressed as:

$$NN(x, y, z) \approx f(x, y, z) \quad (4)$$

The mathematical expression for a neural network is as follows:

$$NN(X) = W_n \sigma_{n-1}(W_{n-1} \sigma_{n-2}(\dots (W_2(W_1 X + b_1) + b_2) + \dots) + b_{n-1}) + b_n \quad (5)$$

And we usually train our neural network by iteratively minimizing a loss function such as Mean Square Error (MSE) in the training dataset (known data). Typically, the MSE loss function, denoted as L_{data} , can be represented as:

$$L_{data} = MSE(NN(x, y, z), f(x, y, z)) = \frac{1}{N_{data}} \sum_{i=1}^{N_{data}} \left(NN(x^i, y^i, z^i) - f(x^i, y^i, z^i) \right)^2 \quad (6)$$

When L_{data} is small enough, we can obtain a well-performing model on the training set. However, when using the model on unseen data, the accuracy can be questionable.

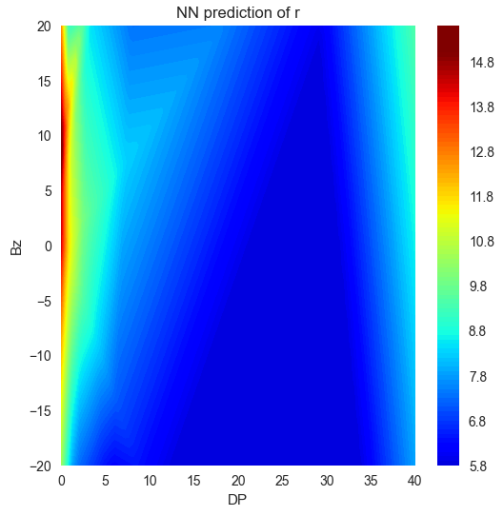


Figure 7. Neural Networks prediction of r

3.3 Regression-based Physics Informed Neural Networks (Reg-PINNs)

The Regression-based Physics Informed Neural Networks (Reg-PINNs) have a similar architecture to vanilla deep forward neural networks. The key difference lies in the MSE loss function, which not only considers the error between the predicted outputs and the known data points but also incorporates the error between the predicted solution by the neural network and the predicted solution by the empirical model. Mathematically, the loss function can be represented as follows:

$$L_{total} = MSE(NN(x, y, z), f(x, y, z)) + MSE(NN(x, y, z), Emp(x, y, z)) \quad (7)$$

The incorporation of empirical models into the framework of Reg-PINNs draws inspiration from the techniques employed in PINNs. It leverage PDEs and ODEs to perform high-resolution simulations in space and time (Raissi, Perdikaris and Karniadakis, 2019). In Reg-PINNs, we utilize the precomputed solutions of algebraic equations to train the model. By combining the high precision of neural networks with the use of traditional empirical models, we significantly enhance the model's generalization capabilities. It is worth mentioning that there is no significant disparity in training time between Reg-PINN and vanilla deep neural network models.

The algorithm and architecture diagram of Reg-PINNs are provided below:

Algorithm 1 Reg-PINNs, Regression-based Physics Informed Neural Networks

Input: - Dataset $D = \{[x_1, x_2, x_3, \dots, x_n] \rightarrow [y_1, y_2, y_3, \dots, y_m]\}$

Output: - Regularized model obtained via the empirical formula (regression form)

Algorithm:

1. Obtain multivariate data.
 2. Calculate $[y_{empirical_1}, y_{empirical_2}, \dots, y_{empirical_m}]$ using the empirical formula.
 3. Implement a Deep Neural Network: $[n \rightarrow n^3 \rightarrow n^2 \rightarrow n \rightarrow m]$ with ReLU activation.
 4. Initialize total Loss to 0.
 5. Set maximum iteration (K), threshold for model ($\epsilon_{threshold}$), learning rate (η)
 6. Initialize model error ϵ (large value) and iteration count to 0.
 7. **While** $\epsilon > \epsilon_{threshold}$ **and** iteration $< K$:
 - A. Obtain predicted outputs $[y_{NN_1}, y_{NN_2}, y_{NN_3}, \dots, y_{NN_4}]$ from the network.
 - B. Calculate MSE loss L_{NN} between $[y_{NN_1}, y_{NN_2}, y_{NN_3}, \dots, y_{NN_m}]$ and $[y_1, y_2, y_3, \dots, y_m]$
 - C. Calculate MSE loss $L_{empirical}$ between $[y_{empirical_1}, y_{empirical_2}, \dots, y_{empirical_m}]$ and $[y_1, y_2, y_3, \dots, y_m]$
 - D. Update total loss: $L_{total} = L_{nn} + L_{empirical}$.
 - E. Update weights using gradient descent and learning rate η .
 - F. Calculate model error: $\epsilon = L_{total}$
 - G. Increment iteration count: $iteration = iteration + 1$
 8. End the algorithm and obtain the regularized model obtained via the empirical formula.
-

The Functional Flow Block Diagram for this research with Reg-PINNs

Proposed Algorithm: (Reg-PINNs)
Regression-based Physics Informed Neural Networks

$$r = r_0 \left(\frac{2}{1 + \cos \theta} \right)^\alpha$$

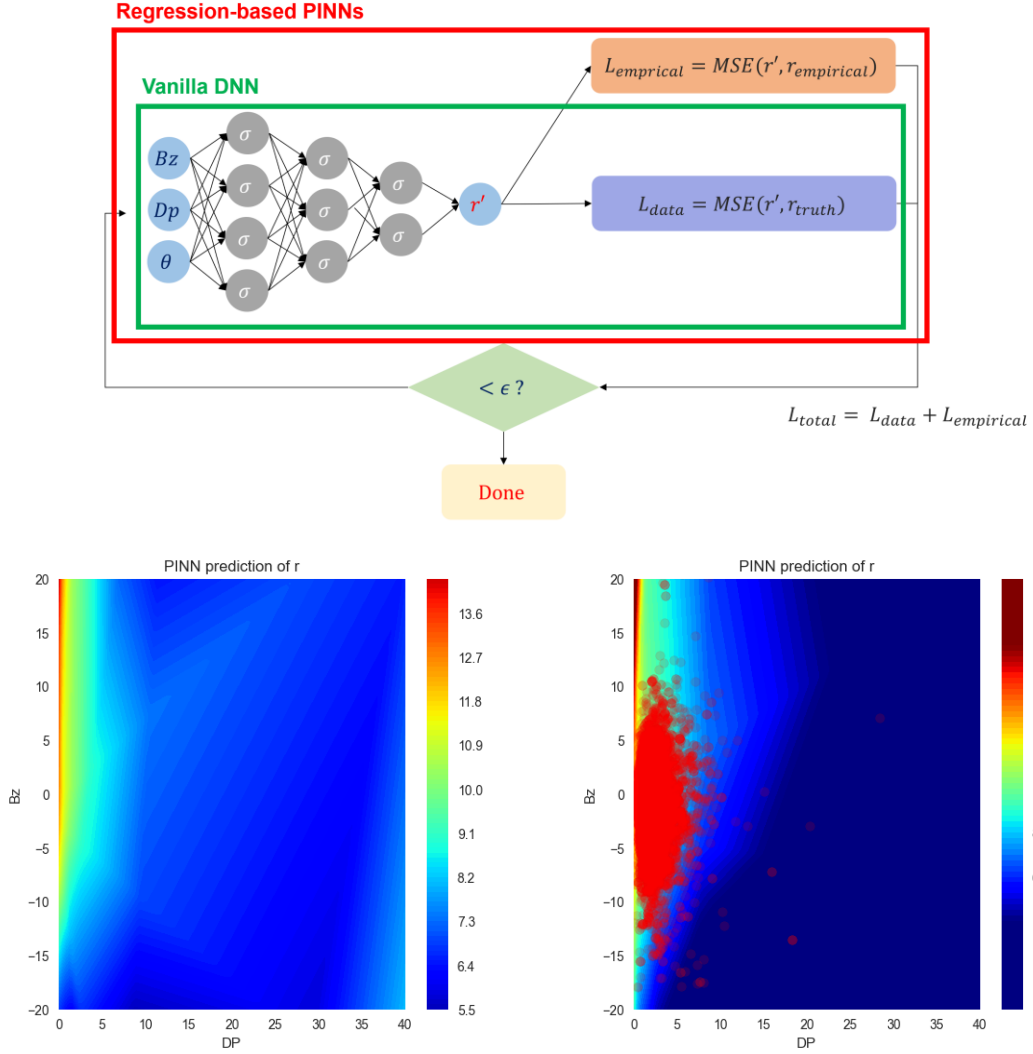


Figure 8. Reg-PINNs (Shue) prediction of r .

Figure 9. Reg-PINNs (Proposed) prediction of r with Dp and Bz distribution.

Figure 8 and Figure 9 illustrate the transformation from a simple neural network to a combined architecture incorporating empirical formulas. In Figure 8, the neural network is combined with the formula from Shue et al. [1998]. It can be observed that the original training results of the neural network (showing a U-shaped pattern as Bz increases) are partially offset by the empirical formula in the region where $Bz > 0$. In Figure 9, it is evident that the results obtained from the proposed empirical function and the neural network training are nearly identical, with only differences in the value range.

4 Results and Discussions

4.1 Overall Evaluation

According to the above information, we evaluate the accuracy of the model using Root Mean Square Error (RMSE). Table 1 presents the RMSE errors obtained from the fitting using the empirical model. The evaluation is performed on two datasets: one includes all data points, and the other is the dataset used by Shue et al. [1998].

Table 1.

Model	RMSE(All)	RMSE(Shue)
Shue et al. [1998] – Baseline	1.22321 Re	1.34754 Re
Proposed Empirical Model	1.19232 Re	1.33783 Re
MCMC	1.19587 Re	1.32348 Re

In Table 1, three rules of thumb are provided. Shue et al. [1998] is used as the baseline, and it can be observed that both the proposed empirical model and MCMC show slight improvements compared to the baseline.

In Table 2, we compare the evaluation of Neural Networks-based models using three types of datasets. The first type involves training the model using all the available data. The second type involves training the model using 80% of the data, and the last type involves training the model using 20% of the data.

Table 2.

Model	RMSE(All)	RMSE(20% unseen)	RMSE(80% unseen)
Shue et al. [1998]	1.22321 Re	1.19798 Re	1.26587 Re
Neural Network	0.85437 Re	0.94781 Re	1.10475 Re
Reg-PINN(Shue)	0.90103 Re	0.92539 Re	0.95703 Re
Reg-PINN(Proposed)	0.91375 Re	0.89304 Re	0.92483 Re

When comparing the training loss, we observe that $L_{NN} < L_{PINN} < L_{Empirical}$. This is because Reg-PINN incorporates the residual of the guiding formula during gradient descent, making the loss higher compared to NN, as shown in Figure 10. Therefore, when evaluating RMSE using the entire dataset, we can see that Neural Network achieves the lowest error. However, as mentioned earlier, machine learning has limited generalization capabilities. Therefore, when introducing the empirical formula, we can observe a significant discrepancy between Reg-PINN, NN, and Shue et al. [1998] in the case of 20% and 80% unseen data. Reg-PINN exhibits robustness and consistently superior accuracy performance compared to NN when evaluated on 20% and 80% unseen data.

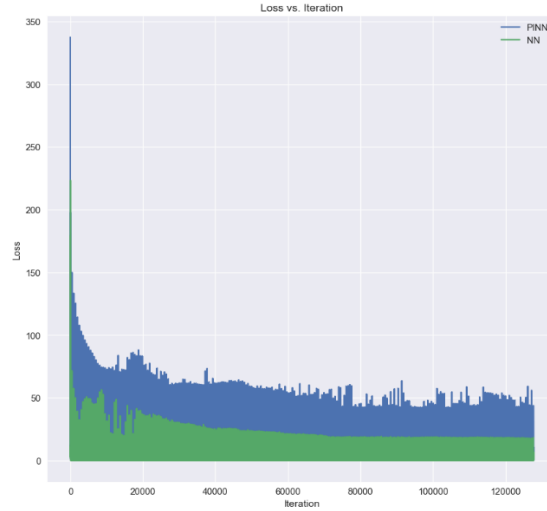


Figure 10. Loss vs Iteration

4.2 Evaluation on different independent variables

In this section, we will individually adjust different variables and explore the varying effects of each model within specific variable ranges. The evaluation in this case is performed using 50% unseen data for testing purposes. Additionally, we introduce L1 (Lasso), L2 (Ridge), and Elastic regularization techniques to enhance the neural network's ability to generalize across different network architectures.

4.2.1 Evaluation on different angles

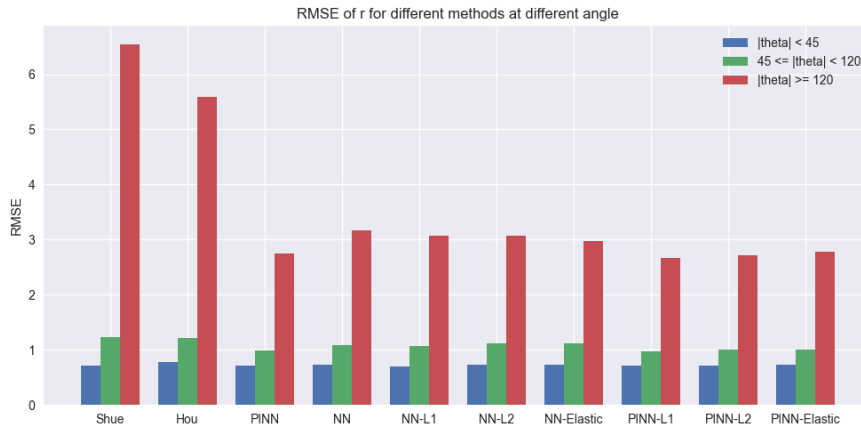


Figure 11. RMSE of r for different methods at different angle

Figure 11 reveals the evaluation of different angular segments ($|\theta| < 45$, $45 \leq |\theta| \leq 120$, $|\theta| > 120$). It is evident that both the Shue model and the proposed empirical model exhibit significant errors in distance estimation for large opening angles. On the other hand, both the NN and the Reg-PINN perform well, with Reg-PINN outperforming NN. For angles smaller than 120 degrees, the performance of all models does not vary significantly.

4.2.2 Evaluation on different IMF Bz

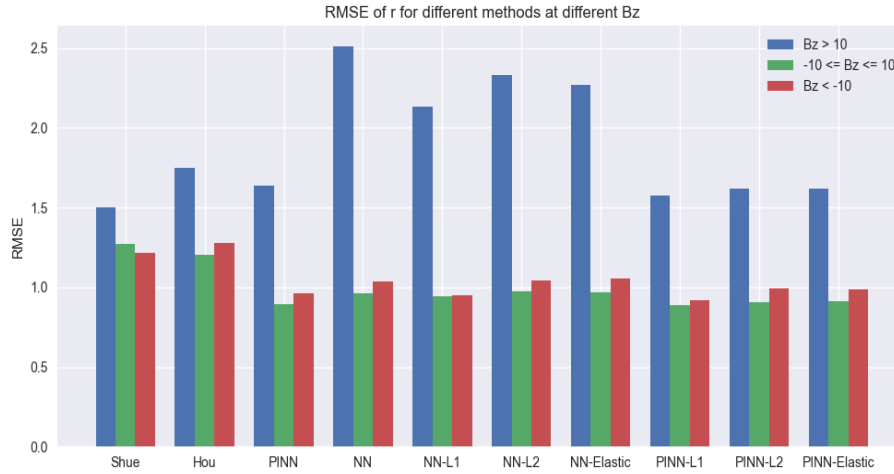


Figure 12. RMSE of r for different methods at different B_z

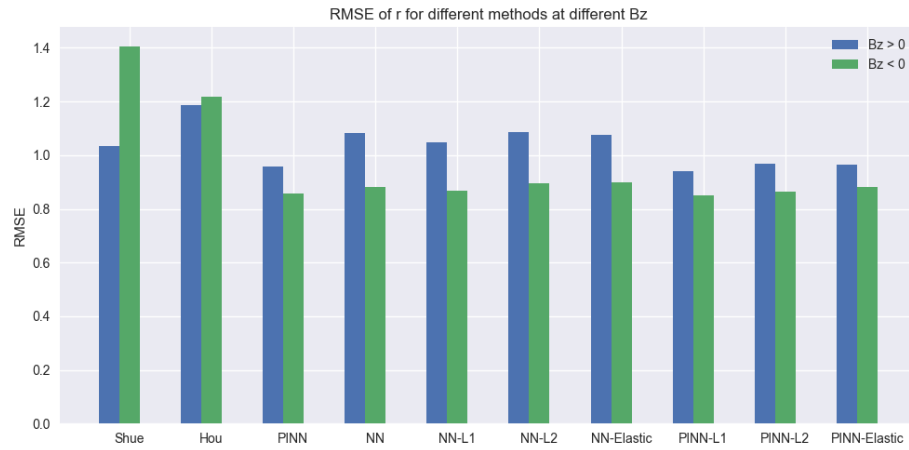


Figure 13. RMSE of r for different methods at different region of B_z

Figure 12 and Figure 13 investigate the ability of the models to handle stronger B_z values and their sensitivity to the north-south interplanetary magnetic field. In Figure 12, it is observed that all types of neural network models perform well when $B_z < 10$. However, as the northward interplanetary magnetic field strength increases, the NN model exhibits significant errors, while Reg-PINN, guided by the empirical formula, maintains low errors even at $B_z > 10$. Overall, Reg-PINN performs the best in this scenario. In Figure 13, it can be seen that all neural network models show poorer response to the northward interplanetary magnetic field. However, Reg-PINN remains the best-performing model among all, especially when incorporating Lasso regularization.

4.2.3 Evaluation on different Dp

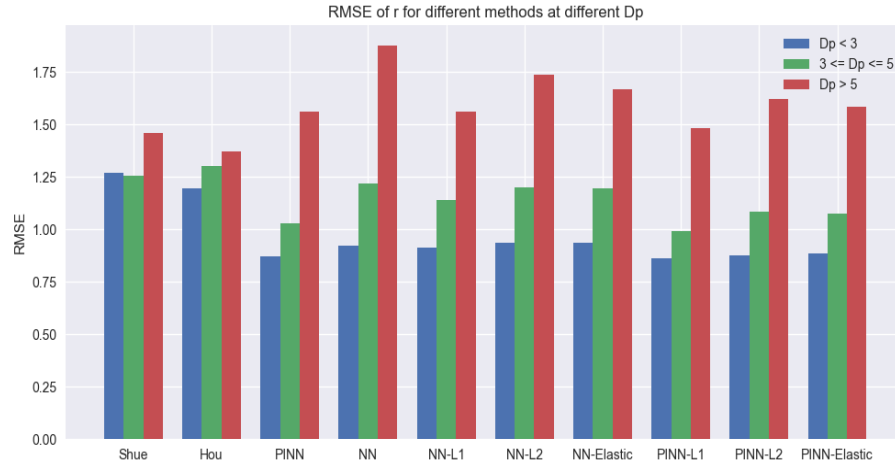


Figure 14. RMSE of r for different methods at different D_p

Figure 14 aims to explore the errors of various models under different solar wind dynamic pressures ($D_p < 3$, $3 \leq D_p \leq 5$, $D_p > 5$). It is evident that as D_p increases, the errors of neural network models also increase. Although they perform reasonably well for $D_p < 5$, only PINN + L1 regularization can compete with Shue et al. [1998] when $D_p > 5$.

4.2.4 Evaluation on Shue et al. [1998] applicable region

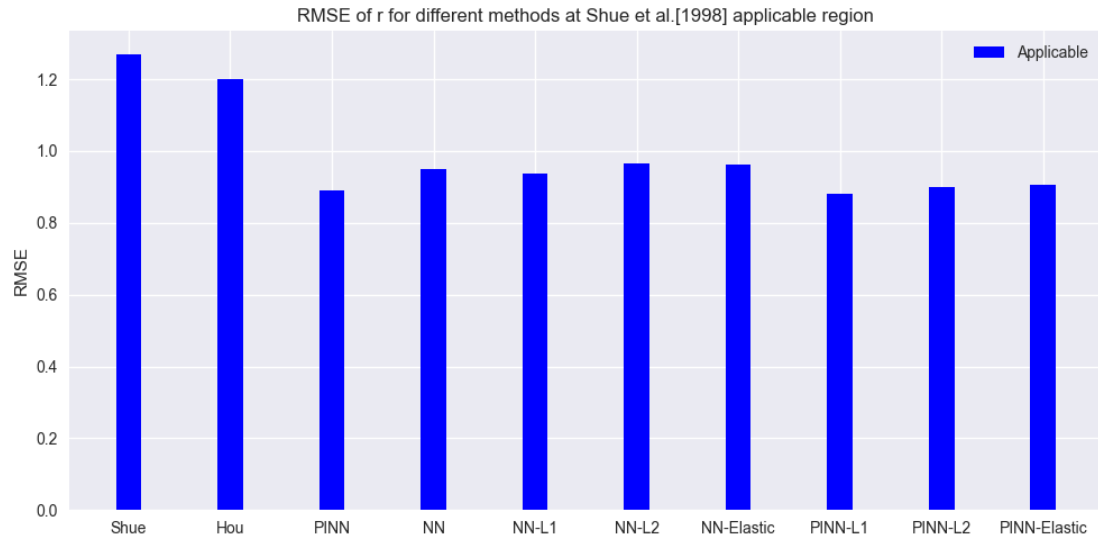


Figure 15. RMSE of r in Shue's applicable region

Figure 15 tests the data points within the applicability range of Shue et al. [1998]. It is evident that the empirical model is unable to compete with the neural network models, while Reg-PINN, benefiting from the guidance of the empirical formula, is less affected by extreme values, allowing the model to generalize well and maintain high accuracy. The RMSE value

for Reg-PINN in Figure 13 is 0.890682, while for Shue et al. [1998], it is 1.269, indicating a reduction in RMSE of approximately 29.8% for Reg-PINN. Notably, the best-performing model in this case is Reg-PINN + L1 with a value of 0.887. This can be attributed to the L1 regularization, which encourages some weights to approach or equal zero, preventing overfitting and enhancing the model's generalization ability. According to the T-test results, we calculated that the p-value for the proposed empirical model, Reg-PINN, compared to Shue et al. [1998] is much smaller than 0.005, indicating a significant difference in the means. On the other hand, the average values between Reg-PINN and NN are closer, with a p-value of 0.698. This suggests that Reg-PINNs is indeed a more accurate and generalizable model constructed based on NN.

5 Conclusions

In conclusion, this paper presents a comprehensive analysis of the relationship between parameters (B_z , D_p) and r_0 and α , proposing alternative empirical models. The proposed algorithm, Reg-PINNs, effectively addresses the limitations of numerical methods and the generalization capabilities of machine learning. The integration of neural networks and empirical models enables the incorporation of low-probability events, including $|B_z| > 10$, $D_p > 5$, $|\theta| > 120$ (each with probabilities of 0.62%, 1.55%, and 1.56% respectively). This combined approach substantially enhances the prediction accuracy for determining the location of the magnetopause within the spatial domain. Reg-PINNs expands the capabilities of traditional PINNs by incorporating algebraic equations for model training, surpassing the scope of ODEs and PDEs. Notably, Reg-PINNs achieves a significant improvement of 29.8% in the accuracy of magnetopause location prediction. In addition, employing L1, L2, and Elastic regularization techniques enhances the prediction of variable r under varying B_z values. We envision that the proposed Reg-PINNs can be applied in various domains, including finance, securities, materials, mechanical engineering, chemistry, and other applied sciences. Reg-PINNs offer the flexibility to integrate domain-specific empirical models alongside neural networks, enabling the modeling and prediction of complex phenomena in different fields. This integration allows researchers and practitioners to leverage the strengths of both empirical models and neural networks, leading to more accurate and robust predictions. The versatility of Reg-PINNs opens new possibilities for advancements in different scientific and practical applications, contributing to the progress and innovation in diverse domains.

List of Acronyms/Abbreviations:

IMF	Interplanetary Magnetic Field
Dp	Dynamic Pressure
NN	Neural Network
PINN	Physics Informed Neural Network
Reg-PINN	Regression-based Physics Informed Neural Network
L1	Lasso
L2	Ridge

Acknowledgements

We would like to express our heartfelt appreciation to Dr. Chun-Yu Lin, Associate Researcher at NCHC – NARLabs, for providing invaluable insights into the concept of Physics Informed Neural Networks and for engaging in fruitful discussions. Additionally, We would like to extend our gratitude to Mr. Yu-Wei Chen and Mr. Pai-Sheng Wang, Researchers at the Space Environment Laboratory – NCU, for their contribution in reinforcing the understanding of magnetopause.

References

- Chao, J.K. *et al.* (2002) ‘Models for the size and shape of the earth’s magnetopause and bow shock’, in L.-H. Lyu (ed.) *COSPAR Colloquia Series*. Pergamon (Space Weather Study Using Multipoint Techniques), pp. 127–135. Available at: [https://doi.org/10.1016/S0964-2749\(02\)80212-8](https://doi.org/10.1016/S0964-2749(02)80212-8).
- J.-H. Shue *et al.* (1998) ‘Magnetopause location under extreme solar wind conditions’, *Journal of Geophysical Research: Space Physics*, 103(A8), pp. 17691–17700. Available at: <https://doi.org/10.1029/98JA01103>.
- Li, S., Sun, Y.-Y. and Chen, C.-H. (2023) ‘An Interpretable Machine Learning Procedure Which Unravels Hidden Interplanetary Drivers of the Low Latitude Dayside Magnetopause’, *Space Weather*, 21(3), p. e2022SW003391. Available at: <https://doi.org/10.1029/2022SW003391>.
- Nemecek, Z. *et al.* (2010) ‘Magnetopause Position Under Different Conditions’, 2010, pp. SM13B-1812.
- Raissi, M., Perdikaris, P. and Karniadakis, G.E. (2019) ‘Physics-informed neural networks: A deep learning framework for solving forward and inverse problems involving nonlinear partial differential equations’, *Journal of Computational Physics*, 378, pp. 686–707. Available at: <https://doi.org/10.1016/j.jcp.2018.10.045>.

Roelof, E.C. and Sibeck, D.G. (1993) 'Magnetopause shape as a bivariate function of interplanetary magnetic field Bz and solar wind dynamic pressure', *Journal of Geophysical Research: Space Physics*, 98(A12), pp. 21421–21450. Available at: <https://doi.org/10.1029/93JA02362>.

Schild, M.A. (1969) 'Pressure balance between solar wind and magnetosphere', *Journal of Geophysical Research (1896-1977)*, 74(5), pp. 1275–1286. Available at: <https://doi.org/10.1029/JA074i005p01275>.

Shue, J.-H. *et al.* (1997) 'A new functional form to study the solar wind control of the magnetopause size and shape', *Journal of Geophysical Research: Space Physics*, 102(A5), pp. 9497–9511. Available at: <https://doi.org/10.1029/97JA00196>.

Speagle, J.S. (2020) 'A Conceptual Introduction to Markov Chain Monte Carlo Methods'. arXiv. Available at: <https://doi.org/10.48550/arXiv.1909.12313>.

Tianping Chen and Hong Chen (1995) 'Universal approximation to nonlinear operators by neural networks with arbitrary activation functions and its application to dynamical systems', *IEEE Transactions on Neural Networks*, 6(4), pp. 911–917. Available at: <https://doi.org/10.1109/72.392253>.

Wang, Y. *et al.* (2013) 'A new three-dimensional magnetopause model with a support vector regression machine and a large database of multiple spacecraft observations', *Journal of Geophysical Research: Space Physics*, 118(5), pp. 2173–2184. Available at: <https://doi.org/10.1002/jgra.50226>.